Spin polarization of electrons tunneling through magnetic-barrier nanostructures

Mao-Wang Lu,[1] Li-De Zhang,[1] and Xiao-Hong Yan[1,2]
[1]*Institute of Solid State Physics, Chinese Academy of Sciences, P.O. Box 1129, Hefei 230031, People's Republic of China*
[2]*Department of Physics, Xiangtan University, Xiangtan, Hunan 411105, People's Republic of China*
(Received 26 September 2002; published 17 December 2002)

We present a theoretical investigation of the spin-dependent transport properties of electrons in nanostructures consisting of realistic magnetic barriers created by a lithographic patterning of ferromagnetic or superconducting films. It is shown that a significant electron-spin polarization effect can be induced by such magnetic-barrier nanostructures with a symmetric magnetic field. It is also shown that an applied bias voltage or an external magnetic field can greatly change the degree of the electron-spin polarization in magnetic-barrier nanostructures. When the applied bias voltage increases, the electron-spin polarization shifts toward the low-energy end and gradually decreases, while, with an increase of the external magnetic field, the electron-spin polarization shifts toward the high-energy direction and successively enlarges. It is also found that the degree of the electron-spin polarization can be tuned with the electric barrier induced by a constant voltage applied to the metallic stripe of system.

DOI: 10.1103/PhysRevB.66.224412 PACS number(s): 75.70.Cn, 73.40.Gk, 73.23.−b

I. INTRODUCTION

Electronic transports in magnetic-barrier nanostructures have attracted considerable attention owing to the advance in the microfabrication technique and its potential applications to electronic devices in recent years.[1–12] Present advances in nanofabrication have made it possible to produce this type of nanostructure, by the deposition of a heterostructure containing a high mobility two-dimensional electron gas (2DEG) in an inhomogeneous magnetic field; for example, microscopic magnetic barriers with amplitudes of several thousand G have been formed in nonplanar devices[3] or by gating a 2DEG with micromagnets[4–6] or superconductors.[7] Experimentally, magnetoresistance oscillations, via the commensurability effect between the classical cyclotron diameter and the period of a magnetic superlattice have been observed.[4,5,7] Very recently, a sharp resistance resonance effect was also observed due to the formation of two types of magnetic edge states.[12] Theoretically, studies of electron tunneling through magnetic barriers[1,2,9] and magnetic superlattices[8] showed that magnetic barriers possess wave-vector filtering, and that magnetic minibands in the energy spectrum are formed in magnetic superlattice.[8]

However, the effect of electron spin on transport properties used to be overlooked. Actually, the spin dependence of the electronic properties of artificial nanostructures is one of today's leading problems in the physics of electronic devices.[13–18] More recently, a few papers called attention to some peculiarities in the dependence of the tunneling probability and the conductance on the electronic spin in magnetic-barrier nanostructures.[19,20] Using a simple δ function magnetic barrier, the effects of intrinsic spin on electronic transport properties were first investigated by Majumdar.[19] It was found that the interaction of the intrinsic spin of a 2DEG with a magnetic field significantly changes the tunneling coefficient and the conductance of electrons. Subsequently, the spin-dependent resonant tunneling of electrons through rectangular and sawtooth magnetic barriers with and without an external electric field was also studied.[20] It was found that certain magnetic barriers can induce the electron-spin polarization effect, and that the electric field can greatly alter the degree of the electron-spin polarization. However, the magnetic barriers used in these studies were not the realistic ones originally proposed by Matulis *et al.*[1] and realized experimentally by Nogaret *et al.*,[12] Carmona *et al.*,[7] and Ye *et al.*[4] For realistic magnetic-barrier nanostructures, electronic transport properties were studied by our group,[2] but the effect of electron spin was not considered. Therefore, in order to reveal the spin-dependent transport properties of realistic magnetic nanostructures, in this paper we employ realistic magnetic barriers instead of ideal ones. The general rule of electron-spin polarization in magnetic barrier nanostructures is revealed. We also investigate the effects of external electric and magnetic fields as well as the electric barrier induced by an applied voltage to the metallic stripes of the system on the electron-spin polarization in the magnetic barrier nanostructures.

II. MODEL AND METHOD

We consider four realistic magnetic barriers[1] labeled (a)–(d), which are formed, respectively, by the deposition, on top of a heterostructure, of a ferromagnetic stripe with magnetization (a) perpendicular and (b) parallel to the 2DEG, (c) of a conduction stripe with a current driven through it, and (d) of a superconducting plate interrupted by a stripe [see Figs. 1(a)–1(d) in Ref. 1]. For these four magnetic-barrier nanostructures, the magnetic fields experienced by the 2DEG in the (x,y) plane are given by

$$\mathbf{B}=B(x,z_0)\hat{z}, \tag{1}$$

$$B(x,z_0)=B_0[K(x+d/2,z_0)-K(x-d/2,z_0)],$$

where (a) $B_0=M_0h/d, K(x,z_0)=2xd/(x^2+z_0^2)$, (b) $B_0=M_0h/d, K(x,z_0)=-z_0d/(x^2+z_0^2)$, (c) $B_0=I/d, K(x,z_0)=\ln[(x^2+z_0^2)/d^2]$, and (d) $B(x,z_0)=B_0\mathrm{Re}[1/\sqrt{1-(x+iz_0)^2}]$. M_0, h, and d are the magnetization, height, and thickness of

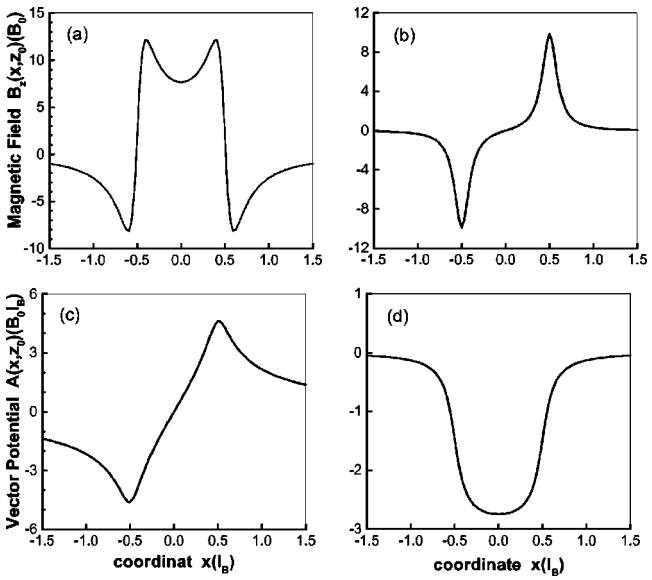

FIG. 1. Two realistic magnetic barriers and their corresponding magnetic vector potentials. Magnetic barriers (a) and (b) are produced by the deposition, on top of a heterostructure, of a ferromagnetic stripe with magnetizations perpendicular and parallel to the 2DEG, respectively, where the structural parameters are chosen to be $d=1$ and $z_0=0.1$, and the magnetic field is in units of B_0.

the stripes, I is the current driven through the stripe, and z_0 is the distance between the stripes and the 2DEG. According to these magnetic-field expressions, these four magnetic barriers can be classified into two groups: symmetric magnetic barriers, $B(-x,z_0)=B(x,z_0)$, containing (a) and (d); and antisymmetric magnetic barriers, $B(-x,z_0)=-B(x,z_0)$, having (b) and (c). For simplicity, we limit our attention to the symmetric magnetic barrier (a) and the antisymmetric one (b); however, our results can also reflect the case of magnetic barriers (c) and (d). Landau magnetic vector potentials $\mathbf{A}(x,z_0)=[0,A(x,z_0),0]$ of magnetic barriers (a) and (b) are given by

$$A(x,z_0)=B_0 d\ \ln\{[(x+d/2)^2+z_0^2]/[(x-d/2)^2+z_0^2]\}$$

and

$$A(x,z_0)=B_0 d\{\arctan[(x-d/2)/z_0]-\arctan[(x+d/2)/z_0]\},$$

respectively. In Figs. 1(a)–1(d), we present these two magnetic barriers and their magnetic vector potentials, where the structural parameters are both chosen to be $d=1.0$ and $z_0=0.1$, the left and right ends of the barriers are assigned as $x_-=-1.5$ and $x_+=1.5$, respectively, and the magnetic field is in units of B_0.

The Hamiltonian for the 2DEG in the above magnetic-barrier nanostructures under a applied bias voltage V_α and an external uniform magnetic field $B_{ex}\hat{z}$ is

$$H=\frac{1}{2m^*}[\mathbf{P}+e\mathbf{A}(x)]^2+\frac{1}{2}\sigma\mu_B g^*[B(x,z_0)+B_{ex}] - \frac{eV_\alpha x}{(x_+-x_-)}, \tag{2}$$

where $\mu_B=e\hbar/2m^*$ is the Bohr magneton, m^* is the effective mass of electron, $\mathbf{P}$ is the momentum of electron, g^* is the effective Lande factor of the electron in a real 2DEG realized using a semiconductor, $\sigma=+1/-1$ is for the up-/down-spin orientation, and $A(x)$ is the total Landau magnetic vector potential consisting of $A(x,z_0)$ of the magnetic barrier and $A_{ex}(x)=B_{ex}[x-(x_++x_-)/2]$ of the external magnetic field. We express quantities in dimensionless units by using the cyclotron frequency $\omega_c=eB_0/m^*$ and the magnetic length $l_B=\sqrt{\hbar/eB_0}$. For GaAs, $g^*=0.44$, $m^*=0.067m_e$ (m_e is the free-electron mass), and an estimated $B_0=0.1T$, we obtain $l_B=81.3$ nm and $\hbar\omega_c=0.17$ meV. Since the problem described by Eq. (2) is translationally invariant along the y direction, the total wave function can be written as a product $\Psi(x,y)=e^{iqy}\psi(x)$, where q is the wave-vector component in the y direction. Accordingly, we obtain the one-dimensional Schrodinger equation

$$\left\{\frac{d^2}{dx^2}-[A(x)+q]^2-\frac{1}{2}g^*\sigma[B(x,z_0)+B_{ex}] + \frac{2eV_\alpha x}{(x_+-x_-)}+2E\right\}\psi(x)=0, \tag{3}$$

where the function $U_\sigma(x,q,V_\alpha,B_{ex})=[A(x)+q]^2/2+g^*\sigma[B(x,z_0)+B_{ex}]/4-eV_\alpha x/(x_+-x_-)$ is usually viewed as the effective potential of the corresponding magnetic nanostructure. Clearly, it depends on the magnetic configuration $B_z(x,z_0)$, the wave-vector component q of the electron in the y direction, the applied bias voltage V_α, the electronic spin σ, and the external magnetic field B_{ex}. Since the effective potential $U_\sigma(x,q,V_\alpha,B_{ex})$ is very complicated, it is impossible to exactly solve Eq. (3). We divide the magnetic-nanostructure region $[x_-,x_+]$ into N ($\gg 1$) segments, each of which has a width $a=(x_+-x_-)/N$, and view the effective potential as a constant $U_\sigma[x_-+(j-0.5)a,q,V_\alpha,B_{ex}]$ in the jth segment $[x_-+(j-1)a,x_-+ja]$. Within this segment, the Schrodinger equation (3) then becomes $\{(d^2/dx^2)-U_\sigma[x_-+(j-0.5)a,q,V_\alpha,B_{ex}]+2E\}\psi(x)=0$, which has the plane-wave solution $\psi_j(x)=c_j e^{ik_j x}+d_j e^{-ik_j x}, x\in[x_-+(j-1)a,x_-+ja]$, where $k_j=\{2E-U_\sigma[x_-+(j-0.5)a,q,V_\alpha,B_{ex}]\}^{1/2}$. In the left and right regions, the wave functions can be written as $\psi(x)=e^{ik_l x}+re^{-ik_l},x<x_-$, and $\psi(x)=te^{ik_r x},x>x_+$, where $k_l=\sqrt{2E-q^2}, k_r=\sqrt{2(E+eV_\alpha)-q^2}$, and r and t are the reflection and transmission amplitudes, respectively. By means of the standard transfer-matrix method, we can obtain

$$\begin{pmatrix} e^{ik_l x_-} & e^{-ik_l x_-} \\ ik_l e^{ik_l x_-} & -ik_l e^{-ik_l x_-}\end{pmatrix}\begin{pmatrix}1\\ r\end{pmatrix} = M\begin{pmatrix} e^{ik_r x_+} & e^{-ik_r x_+} \\ ik_r e^{ik_r x_+} & -ik_r e^{-ik_r x_+}\end{pmatrix}\begin{pmatrix}t\\ 0\end{pmatrix}, \tag{4}$$

where

$$M=\begin{pmatrix} M_{11} & M_{12} \\ M_{21} & M_{22} \end{pmatrix}=\prod_{j=1}^{N}\begin{pmatrix} \cos(k_j a) & -\sin(k_j a)/k_j \\ k_j \sin(k_j a) & \cos(k_j a) \end{pmatrix}$$

is the transfer matrix. Thus the transmission coefficient for spin-electrons tunneling through magnetic barriers can be obtained as follows:

$$T_\sigma(E,q,V_\alpha,B_{ex}) = 4\frac{k_r}{k_l}\left|\left(M_{11}+\frac{k_r}{k_l}M_{22}\right)+i\left(k_r M_{12}-\frac{M_{21}}{k_l}\right)\right|^{-2}. \quad (5)$$

To evaluate the electron spin-polarization effect, it is useful to calculate the spin polarization of the transmitted beam defined by

$$P_T(E,q,V_\alpha,B_{ex})=\frac{T_+(E,q,V_\alpha,B_{ex})-T_-(E,q,V_\alpha,B_{ex})}{T_+(E,q,V_\alpha,B_{ex})+T_-(E,q,V_\alpha,B_{ex})}, \quad (6)$$

where T_+ and T_- are transmission coefficients for spin-up and -down electrons, respectively.

With the transmission coefficient, we calculate ballistic conductance at zero bias and at zero temperature from the well-known Landaur-Buttiker formula, which is given by[1,2]

$$G_\sigma(E_F,B_{ex})=G_0\int_{-\pi/2}^{\pi/2} T_\sigma(E_F,\sqrt{2E_F}\sin\theta,0,B_{ex})\cos\theta d\theta, \quad (7)$$

where θ is the angle between the incidence velocity and the x axis, E_F is the Fermi energy, $G_0=e^2m^*v_F L_y/(2\hbar^2)$, and v_F is the Fermi velocity of electrons. Similar to the electron-spin polarization P_T, we also can define the spin-conductance polarization P_G of the magnetic-barrier nanostructure in terms of the spin conductance G_σ,

$$P_G(E_F,B_{ex})=\frac{G_+(E_F,B_{ex})-G_-(E_F,B_{ex})}{G_+(E_F,B_{ex})+G_-(E_F,B_{ex})}, \quad (8)$$

where G_+ and G_- are the up- and down-spin conductances, respectively.

Under an applied bias V_α, the transmission current I_σ can also be derived from the transmission coefficient T_σ by

$$I_\sigma(V_\alpha)=I_0\int_0^\infty dE\sqrt{E}[f(E,E_F^{left})-f(E,E_F^{right})] \times\int_{-\pi/2}^{\pi/2} T_\sigma(E,\sqrt{2E}\sin\theta,V_\alpha,0)\cos\theta d\theta, \quad (9)$$

where $I_0=L_y e\sqrt{m^*}/2\sqrt{2}\pi^2\hbar^2$ with the structural length L_y in the y direction, and $f(E,E_F^{left})$ and $f(E,E_F^{right})$ are the Fermi-Dirac distribution functions in the left and right electrodes, respectively. When $T=0$ K, Eq. (9) reduces to

$$I_\sigma(V_\alpha)=I_0\int_{E_0}^{E_F} dE\sqrt{E}\int_{-1}^{1} T_\sigma(E,t,V_\alpha,0)dt, \quad (10)$$

where $E_0=(E_F-eV_\alpha)\Theta(E_F-eV_\alpha)$, and Θ is the Heaviside function.

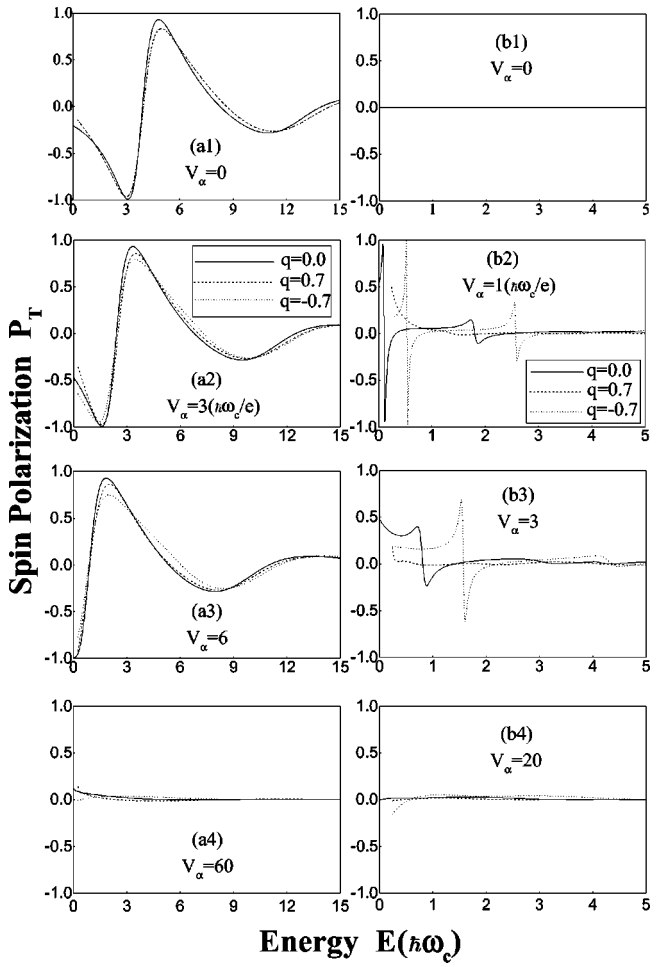

FIG. 2. The spin polarization for electron tunneling through two magnetic-barrier nanostructures at different applied biases, where (a1)–(a4) and (b1)–(b4) correspond to single-barrier (a) and double-barrier (b) magnetic nanostructures with the structural parameters $d=1$, $z_0=0.1$, and $B_0=1$, and V_α is in units of $\hbar\omega_c/e$.

III. RESULTS AND DISCUSSION

Figure 2 shows the spin polarization versus the energy for electrons tunneling through two realistic magnetic-barrier nanostructures produced by depositing ferromagnetic stripes on the surface of the heterostructures with and without applied biases, where the external magnetic field is set to be zero for the moment, i.e., $B_{ex}=0$. One is the single-barrier magnetic nanostructure as presented in Fig. 1(a), while the other is the double-barrier magnetic nanostructure consisting of two identical magnetic barriers, i.e., a barrier presented in Fig. 1(b) is followed by an identical one. Here the structural parameters are both chosen as $d=1$ and $z_0=0.1$, the applied bias V_α is in units of $\hbar\omega_c/e$, and the solid, dashed, and dotted curves correspond to the wave-vector component $q=0.0$, 0.7, and -0.7, respectively. In this figure, the left column [(a1)–(a4)] is the electron-spin polarization for the single-barrier magnetic nanostructure, while the right column [(b1)–(b4)] for the double-barrier one. Without the applied bias $V_\alpha=0.0$ for the double-barrier nanostructure, an electron does not exhibit spin polarization, i.e., $P_T=0$ [see Fig. 2(b1)]. In contrast, the single-barrier nanostructure shows a

considerable electron-spin polarization effect, as depicted in Fig. 2(a1), and the electron-spin polarization P_T is symmetric with respect to the wave vector $q=0$, i.e., the dashed and dotted cures overlap each other. It is well known that the transmission coefficient of particles through a potential is the same as that for particles moving in the opposite direction; in other words, the tunneling characteristics are invariant with respect to the replacement $x\rightarrow -x$ in the equation of motion. Therefore, for the magnetic barrier shown in Fig. 1(b) with an antisymmetric magnetic field $B(x,z_0)=-B(-x,z_0)$ and a symmetric magnetic vector potential $A(x,z_0)=A(-x,z_0)$ [see Figs. 1(b) and 1(d)], at zero-bias voltage the effective potential in Eq. (3) satisfying $U_+(x,q,0,0)=U_-(x,q,0,0)$ results in the transmission coefficient $T_+(E,q,0,0)=T_-(E,q,0,0)$, and thus this type of magnetic-barrier nanostructure does not show the electron-spin polarization. But for the symmetric magnetic barrier presented in Fig. 1(a), $U_+(x,q,0,0)\neq U_-(x,q,0,0)$ due to $B(x,z_0)=B(-x,z_0)$ and $A(x,z_0)=-A(-x,z_0)$ [see Figs. 1(a) and 1(c)], and this kind of magnetic nanostructure therefore exhibits an evident electron-spin polarization effect at zero bias voltage. Under an applied bias voltage, however, the spin-dependent effective potential is greatly altered. For the antisymmetric magnetic barrier, under the applied bias the electrons show a considerable spin polarization [see Figs. 2(b2)–(b4)], and with increasing the bias voltage V_α the electron-spin polarization P_T shifts toward the low-energy region, is gradually weakened, and finally approaches zero. For the symmetric magnetic barrier, under an applied bias the electron-spin polarization is greatly altered due to the variation of the effective potential caused by bias voltage V_α and displays some features similar to antisymmetric magnetic barriers. From Figs. 2(a1)–2(a4), we can clearly see that, when the applied bias increases, the electron-spin polarization P_T also shifts toward the low-energy direction, successively diminishes, and finally disappears. Here it is also interesting to note that for the symmetric magnetic barrier the dependence of the electron wave vector q on the spin polarization is very weak, which is obviously different from that for the antisymmetric magnetic double barriers, due to their different magnetic configurations. From these results, we can conclude that the electron-spin polarization occurs only in symmetric magnetic-barrier nanostructures, and that the applied bias can significantly change its magnitude.

In order to further reveal the effect of an applied bias on the electron-spin polarization, in Fig. 3 we present the transmission current (in units of I_0) versus the applied bias (in units of $\hbar\omega_c/e$) for electrons tunneling through single- and double-barrier magnetic nanostructures given in Figs. 1(a) and 1(b), respectively. The Fermi energy is set to be $E_F=0.6$ (in units of $\hbar\omega_c$), and the structural parameters are the same as in Fig. 2. Here Fig. 3(a) is for the single-barrier case, while Fig. 3(b) is for the double-barrier case, and the solid, dashed, and dotted curves correspond to the without-spin electrons, with up-spin electrons, and with down-spin electrons. There are several prominent features in the I-V_α characteristic that we would like to summarize here. (1) The I-V_α characteristic manifests an obvious negative-differential conductivity effect. (2) When the interaction of the electronic spin with the inhomogenous magnetic field is included, the transmission current is greatly changed (comparing the solid curve with the dashed or dotted one in Fig. 3), and a spin splitting of the transmission current occurs, i.e., the I-V_α characteristic also exhibits an evident spin polarization. (3) The degree of spin polarization of the transmission current depends strongly on the magnetic-barrier configuration and the magnitude of the applied biases. For the symmetric magnetic barrier (a), the I-V_α characteristic exhibits a stronger spin polarization and a sharper peak similar to the transmission coefficient T_σ, while for the antisymmetric magnetic barrier (b) the case is just the opposite.

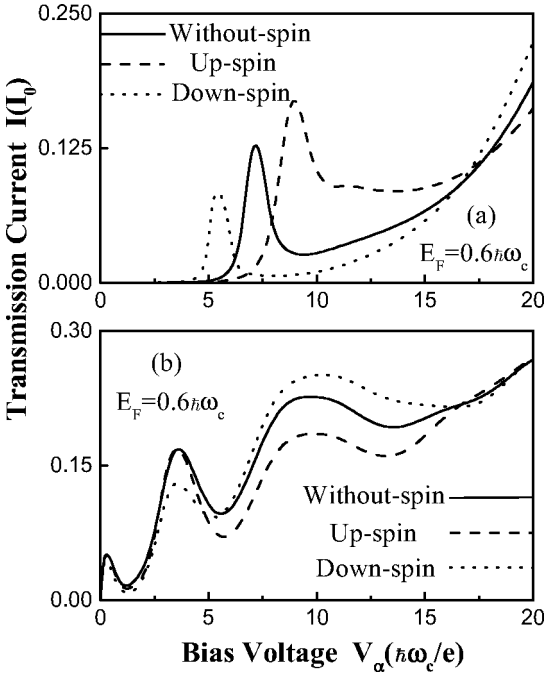

FIG. 3. The transmission current for electron tunneling through two magnetic-barrier nanostructures, where (a) and (b) are for single- and double-barrier magnetic nanostructures with the same structural configuration and parameters as in Fig. 2, respectively.

Next we consider the case in which a uniform magnetic field $B_{ex}\hat{z}$ is further applied to the magnetic-barrier nanostructures to examine the effects of an external uniform magnetic field on spin-dependent transport properties for electrons tunneling through the single barrier given in Fig. 1(a) and the double barriers consisting of two identical magnetic barriers shown in Fig. 1(b), where the structural parameters still are chosen as $d=1$ and $z_0=0.1$ for the two cases. The external magnetic field is in units of B_0, and is assumed not to influence the original magnetic profile of the magnetic barriers, but the total magnetic field experienced by the 2DEG is $\mathbf{B}=[B(x,z_0)+B_{ex}]\hat{z}$. Figure 4 shows that under different external magnetic fields the electron-spin polarization in single-barrier [see Figs. 4(a1)–4(a3)] and double-barrier [see Figs. 4(b1)–4(b3)] magnetic nanostructures, where the structural parameters are the same as in Fig. 3, and the solid, dashed, and dotted curves correspond to the wave vector $q=0.0$, 0.7, and -0.7, respectively. Apparently, with the introducting of an external magnetic field the degree of

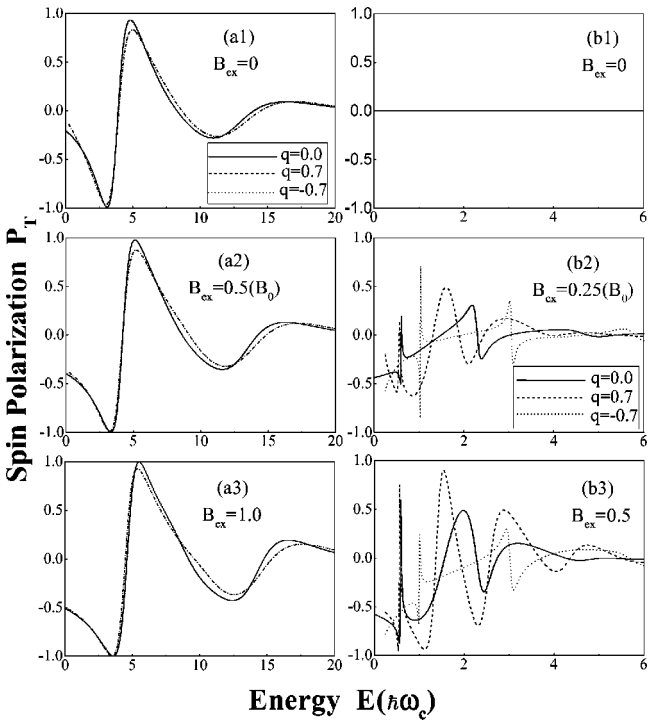

FIG. 4. The spin polarization for electron tunneling through two magnetic-barrier nanostructures at different external magnetic fields, where (a1)–(a4) and (b1)–(b4) correspond to single- and double-barrier magnetic nanostructures with the same structural parameters and configuration as in Fig. 3, respectively, and B_{ex} is in units of B_0.

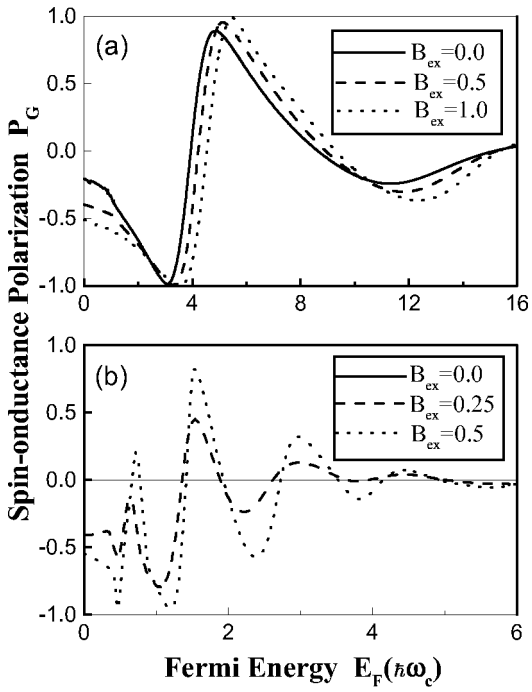

FIG. 5. The spin-conductance polarization for electron tunneling through two magnetic-barrier nanostructures, where (a) and (b) correspond to the single barrier and the double barrier, respectively, and their structural parameters and configurations are the same as in Fig. 4.

the electron-spin polarization of magnetic-barrier nanostructures is significantly altered. For the antisymmetric barrier case, electrons will show an evident spin polarization when the external magnetic field B_{ex} is applied. Moreover, with an increase of the applied magnetic field B_{ex}, the electron-spin polarization shifts to the high-energy region and is strengthened. For the symmetric magnetic-barrier nanostructure, its electron-spin polarization is also changed, and exhibits some features analogous to the antisymmetric magnetic-barrier case as the external magnetic field B_{ex} is applied and increases, but the electron-spin polarization changes slower than that in the asymmetric barrier case. Also, we can see from Figs. 4(a1)–4(a3) that the dashed and dotted curves overlap each other, i.e., for symmetric magnetic barriers the electron-spin polarization is symmetric with respect to the wave vector q, $P_T(E,q,B_{ex})=P_T(E,-q,B_{ex})$. For this type of magnetic barrier under an applied uniform magnetic field, the symmetric total magnetic field $B(x)=B(-x)$ and antisymmetric total magnetic vector potential $A(x)=A(-x)$ lead to an effective potential in the equation of motion [Eq. (3)] having $U_\sigma(x,q,V_\alpha,B_{ex})=U_\sigma(x,-q,V_\alpha,B_{ex})$, so the transmission coefficient $T_\sigma(E,q,V_\alpha,B_{ex})$ is independent of the signs of the wave vector q, and thus P_T is symmetric about q.

Figure 5 shows the results that for different external magnetic fields B_{ex} the spin-conductance polarization versus the Fermi energy without an applied bias at zero temperature, where Figs. 5(a) and 5(b) are for single-barrier and double-barrier magnetic nanostructures, respectively, and their structural parameters are the same as in Fig. 4. Similar to the electron-spin polarization, the spin-conductance polarization is also affected by the applied uniform magnetic field. For the antisymmetric magnetic barrier, at $B_{ex}=0$ the spin-conductance polarization vanishes, i.e., $P_G=0$; under an external magnetic field $P_G\neq 0$, P_G shifts toward the high-Fermi-energy region, and enlarges gradually with an increase of the magnetic field B_{ex}. The same variation of the spin-conductance polarization with the external magnetic field also appears for the symmetric magnetic barrier case [comparing Fig. 5(b) with Fig. 5(a)], but P_G changes more slowly than that for antisymmetric barrier case. These results, presented in both Figs. 4 and 5, imply that one can also change the spin polarization of electrons tunneling through magnetic-barrier nanostructures by the use of an external magnetic field.

Considering that the above results are presented in a dimensionless form, in Fig. 6 we give a quantitative example by using the standard units. Figure 6(a) is the magnetic barrier as shown in Fig. 1(a), where the magnetic field and coordinate are in units of T and nm, respectively, and its structural parameters are chosen to be $d=81.3$ nm, $z_0=8.13$ nm, and $B_0=0.1$ T (which is a typical value). Figure 6(b) corresponds to the electron-spin polarization as a function of the energy and wave vector in this magnetic-barrier nanostructure under both a zero-bias voltage $V_\alpha=0$ and a zero external magnetic field $B_{ex}=0$, where the electronic energy E is in units of meV and the wave vector component q of the electron in the y direction is in units of $1/\mu$m. As

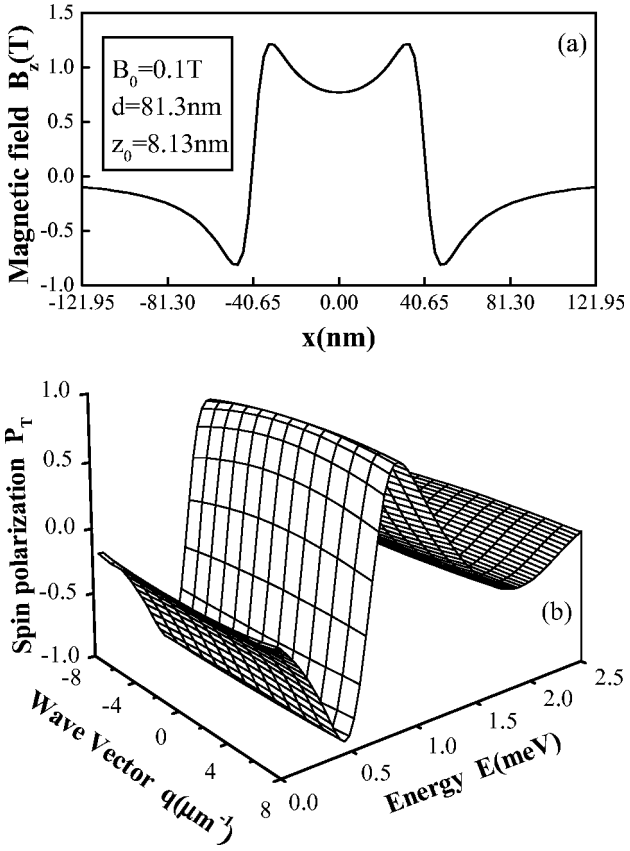

FIG. 6. (a) A realistic magnetic barrier plotted by using units: the magnetic field is in units of T and the coordinate or length in units of nanometers. (b) Its electron-spin polarization as a function of the energy (in units of meV) and the wave vector (in units of μm^{-1}), where the structural parameters are chosen to be $d=81.3$ nm, $z_0=8.13$ nm, and $B_0=0.1$ T.

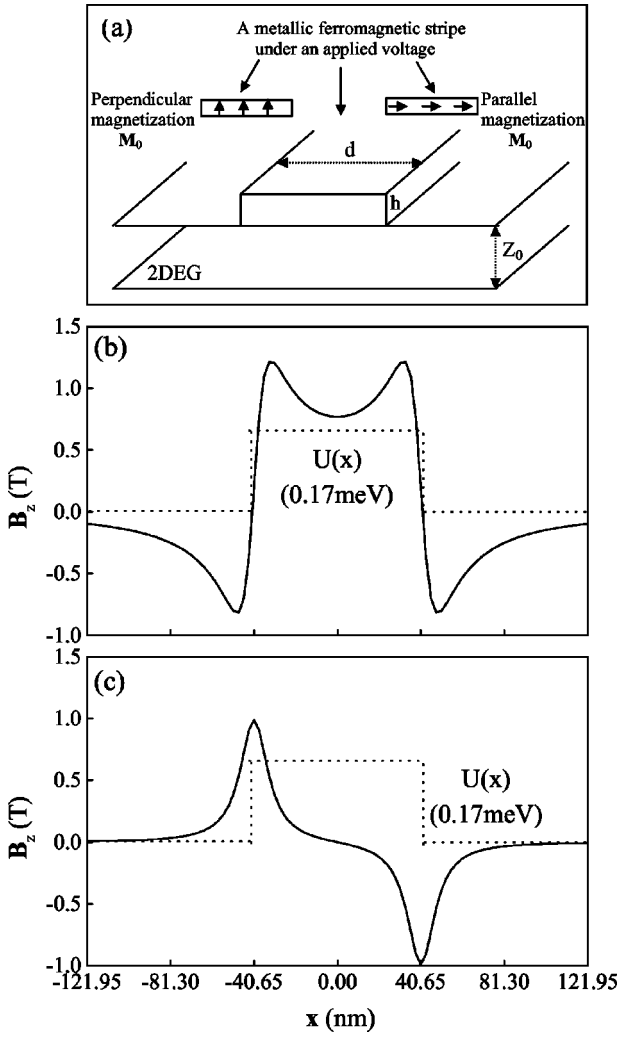

FIG. 7. (a) Schematic illustration of the magnetic-electric-barrier system. (b) and (c) are two magnetic-electric-barrier nanostructures corresponding to a stripe magnetized perpendicularly and parallelly, respectively. Here the structural parameters for these two nanostructures are both chosen to be $B_0=0.1$T, $d=81.3$ nm, $z_0=8.13$ nm, and $x_{\pm}=\pm 121.95$ nm.

discussed above, from Fig. 6(b) we can clearly see that this magnetic barrier exhibits an evident electron-spin polarization effect even at zero-bias voltage and at zero external magnetic field, especially in the low-energy region. Also, one can see that this electron-spin polarization is symmetric with respect to the $q=0$ plane, i.e., $P_T(E,-q)=P_T(E,q)$, which arises from the symmetric magnetic profile $B_z(x,z_0)$ and the antisymmetric magnetic vector potential $A(x,z_0)$ about the x coordinate.

In search of a more efficient control of the electron-spin polarization, we finally consider the case in which a constant voltage is further applied to the ferromagnetic stripes of the system (the stripes are assumed to be metallic). In Fig. 7(a) we schematically depict this kind of system, where the negative (positive) applied voltage will induce an electric barrier (or well),[21,22] together with the magnetic barrier produced by the magnetized stripe. For convenience, we refer to such structures as magnetic-electric barriers, and two magnetic-electric-barrier nanostructures are showed in Figs. 7(b) and 7(c), which correspond to perpendicularly and parallelly magnetized stripes, respectively. Here the electric barrier [the dotted curves in Figs. 7(b) and 7(c)] is viewed as a rectangular shape for simplicity, and it can be expressed by $U(x)=U$ for $-d/2<x<d/2$ and zero otherwise, where the parameter U denotes the electric barrier height or well depth. Note that when the electric barrier appears, the total Hamiltonian of Eq. (2) describing the such hybrid nanostructures is then $H=(1/2m^*)[\mathbf{P}+e\mathbf{A}(x)]^2+\frac{1}{2}\sigma\mu_B g^* B(x,z_0)+U(x)$. In the following, we present numerical results of the electron-spin polarization in magnetic-electric-barrier nanostructures under different electric-barrier heights U.

In Fig. 8 we show the electron-spin polarization P_T as the functions of the energy E and wave vector q through nanostructure given in Fig. 7(b) with different electric-barrier heights (a) $U=0.34$ meV and (b) $U=-0.34$ meV, respectively. Here, the structural parameters are still chosen to be the same as in Fig. 6, i.e., $B_0=0.1T$, $d=81.3$ nm, $z_0=8.13$ nm, and $x_{\pm}=\pm 121.95$ nm. Compared with that of the pure magnetic barrier [see Fig. 6(b)], the electron-spin polarization in hybrid magnetic-electric barrier nanostructures exhibits a few prominent features summarized here. (1) This kind of nanostructure also shows a considerable

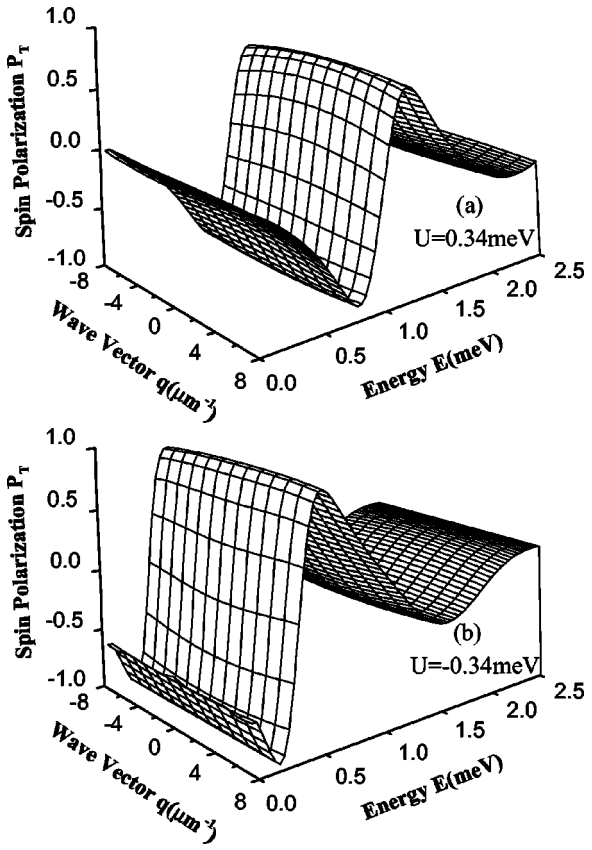

FIG. 8. The electron-spin polarization P_T as functions of the energy E and wave vector q tunneling through the magnetic-electric-barrier nanostructure shown in Fig. 7(b) in the presence of electric barriers (a) $U=0.34$ meV and (b) -0.34 meV, where the structural parameters are chosen to be the same as in Fig. 7(b).

electron-spin polarization effect in the presence of the electric barrier U. (2) Akin to the pure magnetic barrier case, the electron-spin polarization P_T is still symmetric with respect to the $q=0$ plane. This is because the spin-dependent transmission coefficient T_σ is symmetric about the plane $q=0$ due to the symmetry of the electric barrier $U(x)$ about x for this kind of magnetic-electric-barrier nanostructure. That is to say, the presence of the electric barrier does not change the symmetry of the electron-spin polarization with respect to the wave vector q. (3) However, the electron-spin polarization P_T is closely associated with the applied voltage to the metallic stripe of system or the electric barrier U , namely, the electric barrier U can greatly changes the degree of the electron-spin polarization. When a negative voltage is applied to the stripe (i.e., $U>0$), P_T shifts towards the high-energy end and reduces; while it moves in the low-energy direction and increases for a positive applied voltage (i.e., $U<0$). This is expected from the variation of the effective potential induced by the applied voltage, and means that one can efficiently control the electron-spin polarization by tuning the voltage applied to the stripe of the system. Regarding the magnetic-electric barrier nanostructure shown in Fig. 7(c), it does not possess any electron-spin splitting of the transmission no matter if the electric barrier parameter is $U=0$ or $U\neq 0$. This occurs because for this nanostructure the

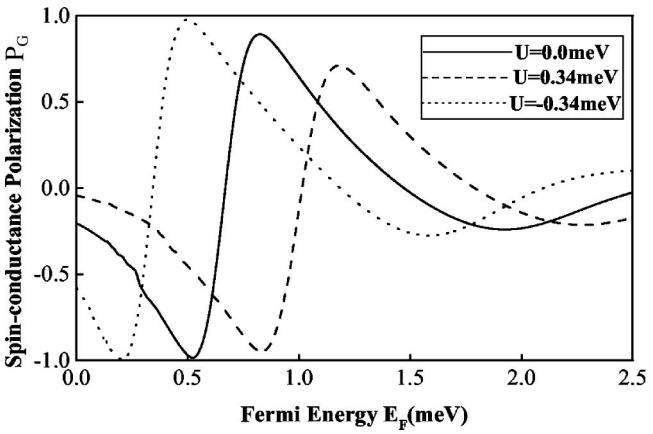

FIG. 9. The spin-conductance polarization or the relative spin-conductance excess P_G as a function of the Fermi energy E_F for the magnetic-electric-barrier nanostructure given in Fig. 7(b) with different electric-barrier heights $U=0$ (solid curve), 0.34 meV (dashed curve), and -0.34 meV (dotted curve), where the structural parameters are the same as in Fig. 8.

magnetic field $B_z(x)$ and the corresponding magnetic vector potential $A(x)$ [the electric barrier $U(x)$ as well] are antisymmetric and symmetric with respect to the coordinate x, respectively, i.e., $B_z(-x)=-B_z(x)$ and $A(-x)=A(x)$ as well as $U(-x)=U(x)$. As a consequence of this, the spin-dependent effective potentials in Eq. (3) satisfy $U_+=U_-$, according to the well-known fact that the transmission coefficient through a potential barrier is equal for particles moving in opposite directions (i.e., the tunneling characteristics are invariant with respect to the replacement $x\rightarrow -x$ in the equation of motion). Indeed, our calculations also substantiate the electron-spin polarization $P_T=0$ for this kind of magnetic-electric barrier nanostructures.

Figure 9 shows the results of the spin-conductance polarization P_G (or the relative spin conductance excess) versus the Fermi energy E_F for spin electrons tunneling through the magnetic-electric barrier nanostructure presented in Fig. 7(b), where the structural parameters are still chosen to be the same as in Fig. 8. In this figure the solid, dashed, and dotted curves are for the electric-barrier heights $U=0$, 3.4, and -3.4 meV , respectively. From this figure, it is obvious that the spin-conductance polarization P_G exhibits features similar to the electron-spin polarization P_T with the electric-barrier height U. For the electric barrier $U>0$, the spin-conductance polarization P_G moves toward in high-Fermi-energy region and diminishes, while it shifts toward the low-Fermi-energy region and increases for the electric potential well $U<0$. These features reflected in the spin-conductance polarization indicate again that one can manipulate the spin-polarized electrons in semiconductors by using an electric barrier, i.e., by means of tuning the applied voltage to the metallic stripe of the system.

IV. CONCLUSIONS

In summary, we have studied the electron-spin polarization in the realistic magnetic-barrier nanostructures. It is

shown that only in symmetric magnetic-barrier nanostructures do electrons display an evident spin polarization effect. It is also shown that an applied bias or an external magnetic field can greatly affect the degree of electron-spin polarization in such magnetic-barrier nanostructures. The electron-spin polarization shifts toward the low-energy region and diminishes when an applied bias voltage increases, while, as an external magnetic field increases, the electron-spin polarization shifts towards the high-energy region and is successively enhanced. If the ferromagnetic stripes of the system are metallic, one can apply a constant voltage to stripes, and this voltage will further induce a electric barrier together with the magnetic barrier, i.e., forming a so-called hybrid magnetic-electric barrier structure. The electron-spin polarization in magnetic-barrier nanostructures is found to be strongly dependent upon the electric-barrier height or the applied voltage on the metallic stripes. These results obtained in this paper summarize the general rule of electron-spin polarization in magnetic-barrier nanostructures, and imply that one can control the degree of spin polarization of electrons tunneling through magnetic-barrier nanostructures by means of an external electric field, an external magnetic field, as well as an electric barrier induced by an applied voltage of strips of the system, which can be useful for the design and applications of magnetic-barrier-based spintronic devices.

ACKNOWLEDGMENTS

This work was supported by the National Major project of Fundamental Research: Ministry of Sciences and Technology of China under Grant No. 1999064501 and by the National Natural Science Foundation of China under Grant No. 10074064.

[1] A. Matulis, F. M. Peeters, and P. Vasilopoulos, Phys. Rev. Lett. **72**, 1518 (1994).
[2] J. Q. You, Lide Zhang, and P. K. Ghosh, Phys. Rev. B **52**, 17 243 (1995).
[3] M. L. Leadbeater, C. L. Foden, J. H. Burroughes, M. Pepper, T. M. Burke, L. L. Wang, M. P. Grimshaw, and D. A. Ritchie, Phys. Rev. B **52**, R8629 (1995).
[4] P. D. Ye, D. Weiss, R. R. Gerhardts, M. Seeger, K. von Klitzing, K. Eberl, and H. Nickel, Phys. Rev. Lett. **74**, 3013 (1995).
[5] M. Kato, A. Endo, S. Katsumoto, and Y. Iye, Phys. Rev. B **58**, 4876 (1998).
[6] V. Kubrak, F. Rahman, B. L. Gallagher, P. C. Main, and M. Henini, C. H. Marrows, and M. A. Howson, Appl. Phys. Lett. **74**, 2507 (1999); F. M. Peeters and X. Q. Li, *ibid.* **72**, 572 (1998).
[7] H. A. Carmona, A. K. Geim, A. Nogaret, P. C. Main, T. J. Foster, M. Henini, S. P. Beaumont, and M. G. Blamire, Phys. Rev. Lett. **74**, 3009 (1995).
[8] I. S. Ibrahim and F. M. Peeters, Phys. Rev. B **52**, 17 321 (1995); A. Krakovsky, *ibid.* **53**, 8469 (1996); Z. Y. Zeng, L. D. Zhang, X. H. Yan, and J. Q. You, *ibid.* **60**, 1515 (1999).
[9] Yong Guo, Bing-Lin Gu, Wen-Hur Duan, and Yu. Zhang, Phys. Rev. B **55**, 9314 (1997).
[10] A. Nogaret, S. Carlton, B. L. Gallagher, P. C. Main, M. Henini, R. Wirtz, R. Newbury, M. A. Howson, and S. P. Beaumont, Phys. Rev. B **55**, R16037 (1997).
[11] A. Matulis and F. M. Peeters, Phys. Rev. B **62**, 91 (2000).
[12] A. Nogaret, S. J. Bending, and M. Henini, Phys. Rev. Lett. **84**, 2231 (2000).
[13] B. E. Kane, Nature (London) **393**, 133 (1998); G. A. Prinz, Science **282**, 1660 (1998); Phys. Today **48**(4), 58 (1995).
[14] Can-Ming Hu, Junsaka Nitta, Tatsushi Akazaki, Jiro Osaka, P. Pfeffer, and W. Zawadzki, Phys. Rev. B **60**, 7736 (1999); D. Richards and B. Jusserand, *ibid.* **59**, R2506 (1999); A. V. Moroz and C. H. W. Barnes, *ibid.* **61**, R2464 (2000).
[15] D. P. Divincenzo, Nature (London) **393**, 113 (1998).
[16] P. Khandelwal, N. N. Kuzma, S. E. Barrett, L. N. Pfeiffer, and K. W. West, Phys. Rev. Lett. **81**, 673 (1998).
[17] C. Mathieu, J. Jorzick, A. Frank, S. O. Demokritov, A. N. Siavin, and B. Hillebrands, Phys. Rev. Lett. **81**, 3968 (1998); O. Steffens and M. Suhrke, *ibid.* **82**, 3891 (1998).
[18] E. A. de Andrada e Silva and G. C. La Rocca, Phys. Rev. B **59**, R15583 (1999); P. Pfeffer and W. Zawadzki, *ibid.* **59**, R5312 (1999); O. Voskoboynikov, C. P. Lee, and O. Tretyak, *ibid.* **63**, 165306 (2001).
[19] A. Majumdar, Phys. Rev. B **54**, 11 911 (1996).
[20] V. N. Dobrovolsky, D. I. Sheka, and B. V. Chernyachuk, Surf. Sci. **397**, 333 (1998); Yong Guo, Bing-Lin Gu, Zhong Zeng, Jing-Zhi Yu, and Yoshiyuki Kawazoe, Phys. Rev. B **62**, 2635 (2000).
[21] G. Papp and F.M. Peeters, Appl. Phys. Lett. **78**, 2184 (2001); **79**, 3198 (2001).
[22] H. Z. Xu and Y. Okada, Appl. Phys. Lett. **79**, 3119 (2001).